Reduced inverse Born series: a computational study

VADIM A. MARKEL[1] [iD] **AND JOHN C. SCHOTLAND**[2,*] [iD]

[1]*Department of Radiology, University of Pennsylvania, Philadelphia, Pennsylvania 19104, USA*
[2]*Department of Mathematics and Department of Physics, Yale University, New Haven, Connecticut 06511, USA*
Corresponding author: john.schotland@yale.edu

We investigate the inverse scattering problem for scalar waves. We report conditions under which the terms in the inverse Born series cancel in pairs, leaving only one term at each order. We refer to the resulting expansion as the reduced inverse Born series. The reduced series can also be derived from a nonperturbative inversion formula. Our results are illustrated by numerical simulations that compare the performance of the reduced series to the full inverse Born series and the Newton–Kantorovich method.   © 2022 Optica Publishing Group

1. INTRODUCTION

The inverse scattering problem (ISP) is of fundamental importance in optics and nearly every branch of physics. There are numerous applications in fields ranging from biomedical imaging to atmospheric science, and extending over spatial scales from microscopic to macroscopic. The problem is usually stated in the following form: determine the scattering potential of a medium of interest from measurements of the scattered field. The scattering potential is related to the dielectric permittivity in optics, the speed of sound in acoustics, and corresponds to the potential energy of a particle in quantum mechanics. There are a number of approaches to reconstruct the scattering potential. Direct reconstruction methods provide an analytic solution to the ISP, principally in 1D, although higher-dimensional methods are also known. Nonlinear optimization, which is often based on Newton's method and its variants, is extremely flexible, but has high computational complexity. A comprehensive overview of inverse scattering theory can be found in [1].

In a landmark paper, Wolf pioneered the study of the ISP for scalar waves, motivated by applications in optical imaging [2]. He derived an inversion formula for the linearized ISP in a transmission experiment. This formula holds within the accuracy of the first Born approximation. In later work, Wolf extended this result to a nonlinear ISP by using a direct reconstruction method that is now known as the inverse Born series (IBS) [3].

The IBS was initially developed for the 1D quantum mechanical ISP [4]. Later, it was extended to higher dimensions and to a variety of ISPs in classical and quantum physics [5,6]. These include the ISPs of optical tomography, electrical impedance tomography, and acoustic and electromagnetic imaging [7–15]. The convergence of the IBS has been analyzed in [16–18]. We note that the computational advantage of the IBS is that it does not require evaluation of the forward operator. However, the number of terms in the IBS grows exponentially, which limits its use to weakly nonlinear problems. A survey of these developments can be found in [19].

In this paper, we apply the IBS to an ISP for scalar waves. The scattering potential is assumed to have compact support, so that the corresponding Lippmann–Schwinger integral equation can be discretized in a finite volume, thereby becoming a system of linear algebraic equations. In this setting, the ISP is discrete, and consists of finding the susceptibilities of the volume elements in the discretization. The corresponding IBS is algebraic and is amenable to straightforward analysis. We find that there is a cancellation of terms, in which exponentially many terms cancel in pairs, with a single term remaining at each order. We refer to the resulting series as the reduced inverse Born series (rIBS). Under certain conditions (single source or detector), the cancellations are exact and the rIBS and IBS coincide. In this setting, the rIBS can also be derived from a nonperturbative inversion formula. In other cases, the rIBS can be viewed as an approximation. Numerical simulations of 1D and 2D scatterers embedded in 3D space are used to illustrate the applicability of the rIBS. Throughout, we compare reconstructions obtained with the IBS, rIBS, and the Newton–Kantorovich (NK) methods. The NK method is a variant of Newton's method that does not require computation of a derivative for every iterative step [20]. We consider separately: (i) The case when the rIBS is exact, (ii) the case when the IBS and NK methods are exact, but the conditions for the applicability of rIBS are not met, and (iii) the case when all methods fail. For simplicity, we restrict our attention to scalar waves, but the generalization to the case of vector electromagnetic fields is straightforward.

The remainder of this paper is organized as follows. The necessary theoretical background is introduced in Section 2. The rIBS and the accompanying nonperturbative inversion formula are derived in Section 3. 1D and 2D numerical examples are shown in Sections 4 and 5. Finally, Section 6 contains a discussion of our results.

Throughout the paper we use the following notational conventions. Matrices are denoted by straight typewriter-style letters such as A. Matrix elements are denoted by italic letters as in A_{nm}. If a matrix is diagonal, its elements are denoted by small italic letters; for example, a diagonal matrix V has elements $V_{nm} = v_n \delta_{nm}$.

2. NONLINEAR INVERSE SCATTERING PROBLEM

A. General Formulation

We consider the scattering theory for a scalar field. Rather than beginning with the wave equation, we introduce an equivalent formulation in terms of integral equations [21]. The forward problem is to determine the scattered field from the scattering potential. The corresponding inverse problem is to recover the potential from measurements of the scattered field. In both problems, the T matrix plays a crucial role. Consider the field generated by a monochromatic point source at the location $\mathbf{r}_s$, and let the point of observation be $\mathbf{r}_d$. We denote the field measured in such an experiment by $\Phi(\mathbf{r}_d, \mathbf{r}_s)$. The connection to the T matrix is established by the integral equation

$$\int_\Omega \mathrm{d}^3 r \int_\Omega \mathrm{d}^3 r' \, G(\mathbf{r}_s, \mathbf{r}) T(\mathbf{r}, \mathbf{r}') G(\mathbf{r}', \mathbf{r}_d) = \Phi(\mathbf{r}_s, \mathbf{r}_d), \quad (1)$$

where Ω is the region containing the scatterer, $T(\mathbf{r}, \mathbf{r}')$ is the kernel of the T matrix operator and $G(\mathbf{r}, \mathbf{r}')$ is the free-space Green's function. The operator T is defined by

$$T = V + TGV = V + VGT, \quad (2)$$

where V is the scattering potential. The equation above can be formally solved for T by

$$T = V(I - VG)^{-1} = (I - VG)^{-1}V, \quad (3)$$

where I is the identity operator. Note that V is diagonal by definition, which means that its kernel is of the form $V(\mathbf{r}, \mathbf{r}') = v(\mathbf{r}) \delta(\mathbf{r} - \mathbf{r}')$. Here, $v(\mathbf{r})$ refers, for example, to the dielectric susceptibility of the scattering medium. In general, $v(\mathbf{r})$ vanishes outside of the scatterer. We also assume that the sources and detectors are located outside of Ω, which contains the support of $v(\mathbf{r})$. Note that the principle of reciprocity implies that $T(\mathbf{r}, \mathbf{r}') = T(\mathbf{r}', \mathbf{r})$, so that T is symmetric.

By expanding the right hand side of Eq. (2), we obtain a series for T in powers of V that is given by

$$T = V + VGV + VGVGV + \cdots. \quad (4)$$

We will refer to Eq. (4) as the Born series.

In practice, a computational implementation of a reconstruction method uses a finite amount of data. As a result, a reconstruction algorithm produces an approximation to a continuously varying scattering potential. Here, we approximate the potential in a basis of functions that are constant on volume elements of Ω. To this end, we discretize the integral Eq. (1) as follows. Suppose that there are N_s sources, N_d detectors, and N_v volume elements in Ω. Let $A_{in} = G(\mathbf{r}_{si}, \mathbf{r}_n)$, $T_{nm} = T(\mathbf{r}_n, \mathbf{r}_m)$, $B_{mj} = G(\mathbf{r}_m, \mathbf{r}_{dj})$, and $\Phi_{ij} = \Phi(\mathbf{r}_{si}, \mathbf{r}_{dj})$, where $i = 1, \ldots, N_s$, $j = 1, \ldots, N_d$, and $n, m = 1, \ldots, N_v$. Replacing the integral by a sum, Eq. (1) becomes

$$\sum_{n,m} A_{in} T_{nm} B_{mj} = \Phi_{ij}, \quad (5)$$

which we write in the form

$$\mathrm{AT[V]B} = \Phi, \quad (6)$$

where the dependence of the matrix T on V has been made explicit. Note that the incident and measured fields will correspond to discrete sets of sources and detectors, but we relax the assumption that the latter are points. We can, for example, consider illumination by several distinct plane waves. We will refer to A and B as measurement matrices since they establish the linear relation between the scattering potential and the data. Specific forms of A and B depend on the illumination and detection schemes and several examples are given below. In addition, we note that in Eq. (6), V is a diagonal matrix with the elements $V_{nm} = v_n \delta_{nm}$. We also note that it is possible to set $G_{nn} = 0$ for all n, so that the matrix G has a zero diagonal [22]. We assume that this is the case below.

The ISP can now be formulated as follows: Given the matrix of data Φ, find the diagonal matrix V that solves Eq. (6). Since T depends nonlinearly on V, this is a nonlinear problem. As discussed in the next section, the first step is to consider the linearization of this problem.

B. Linearization

While this paper is focused on solving the nonlinear ISP, we will frequently need a solution to the corresponding linearized problem, which we denote by L. Here, L denotes the solution to

$$\mathrm{ALB} = \Phi. \quad (7)$$

Note that L is diagonal by definition and we denote its elements by ℓ_n. If it is known a priori that V is small in norm, then L is a good approximation to the solution to the ISP. However, we are interested in situations where this approximation is not accurate.

The two-sided matrix multiplication in Eq. (7) together with the condition that L is diagonal defines a linear operator $\mathcal{K}$. Equation (7) can be rewritten as

$$\mathcal{K}\mathrm{L} = \Phi. \quad (8)$$

The operator $\mathcal{K}$ acts on square diagonal matrices of size $N_v \times N_v$ and returns a matrix of size $N_s \times N_d$. For a diagonal matrix D with elements d_n, $\mathcal{K}$ is defined by

$$(\mathcal{K}\mathrm{D})_{ij} = \sum_{n=1}^{N_v} K_{(ij),n} d_n \quad \text{where} \quad K_{(ij),n} = A_{in} B_{nj}. \quad (9)$$

Note that $\mathcal{K}$ can be rearranged into an $N_s N_d \times N_v$ matrix K. The latter can be viewed as acting on vectors of length N_v and

returning a vector of length $N_s N_d$. The two formulations of the linearized problem (using the operator $\mathcal{K}$ or the matrix K) are equivalent. However, working with K as with a generic matrix disregards the algebraic structure, which is explicit in the second part of Eq. (9). As was shown in [23,24], accounting for this structure results in a more efficient reconstruction algorithm.

Equation (8) may not have a solution. When a solution does not exist or is not unique, we seek the pseudo-inverse solution of Eq. (8) instead. This allows the number of linearly independent equations in Eq. (8) to be larger or smaller than the number of unknowns ℓ_n. The operator $\mathcal{K}$ has a pseudoinverse, which we denote by $\mathcal{K}^+$. This operator acts on a matrix of size $N_s \times N_d$ and returns a diagonal matrix of size $N_v \times N_v$. Thus L can be written in the form

$$L = \mathcal{K}^+ \Phi. \tag{10}$$

Efficient numerical methods to compute $\mathcal{K}^+$ for domains Ω with translational symmetry (such as a slab or a cylinder) have been described in [25] and for regions without such symmetry in [23,24].

C. Inverse Born Series

The IBS is derived by acting with $\mathcal{K}^+$ on the nonlinear Eq. (6), which results in

$$\mathcal{K}^+(AT[V]B) = L. \tag{11}$$

Using the relation in Eq. (2) in Eq. (11), we find that

$$(\mathcal{K}^+\mathcal{K})V = L - \mathcal{K}^+(A\,T[V]\,G\,V\,B). \tag{12}$$

If we substitute $\mathcal{K}^+\mathcal{K} = I$ on the left-hand side of the above equation, we obtain

$$V = L - \mathcal{K}^+(A\,T[V]\,G\,V\,B). \tag{13}$$

If $\mathcal{K}^+\mathcal{K} \neq I$, then the quantity on the left-hand side of Eq. (13) is the projection of V onto the subspace on which $\mathcal{K}$ is invertible. After making use of the forward Born series for T[V] in matrix form, Eq. (13) becomes

$$V = L - \mathcal{K}^+[A\,(VGV + VGVGV + VGVGVGV + \cdots)\,B]. \tag{14}$$

Suppose that

$$V = V^{(1)} + V^{(2)} + V^{(3)} + \cdots, \tag{15}$$

where $V^{(p)}$ contains p factors of L [see Eq. (16) below]. Substituting Eqs. (15) into Eq. (14) and matching powers of L, we find that

$$V^{(1)} = L,$$

$$V^{(2)} = -\mathcal{K}^+[A(V^{(1)}GV^{(1)})B],$$

$$V^{(3)} = -\mathcal{K}^+[A\left(V^{(1)}GV^{(2)} + V^{(2)}GV^{(1)} + V^{(1)}GV^{(1)}GV^{(1)}\right)B]. \tag{16}$$

We will refer to Eq. (15) as the IBS. At each order $p > 1$, the term $V^{(p)}$ can be computed recursively using compositions of the integer p and the previously computed terms of orders less

than p. We note that the number of terms in the IBS grows exponentially with p. Therefore, computing the series to a high order is prohibitively computationally expensive.

D. NK method

The NK method is an iterative procedure to solve the ISP. It is derived by noting that Eq. (12) leads to the fixed-point iteration

$$V_{p+1} = L - \mathcal{K}^+(A\,T[V_p]\,G\,V_p\,B), \quad V_1 = L. \tag{17}$$

It is important to note that the iterations in Eq. (17) require solving the forward problem (computing $T[V_p]$) at each order, which is computationally expensive. The IBS method bypasses this difficulty by using a series expansion for T[V]. We also note that if the IBS and NK method both converge, they have the same limit [12]. The convergence of the IBS has been investigated in [16,18].

3. REDUCED INVERSE BORN SERIES

In this section, we study a remarkable cancellation of terms in the IBS that occurs for the ISP with a single detector. Consider a formally determined ISP specified by a square invertible matrix A of size $N \times N$, where $N = N_s = N_v$. We suppose that the measurement matrix B consists of just one column of length N_v with all entries constant, which we take to be equal to 1. Under the above conditions, Eq. (5) becomes

$$\sum_m (AT[V])_{im} = \Phi_{i1}. \tag{18}$$

The corresponding linearized equation is of the form

$$\sum_m A_{im}\ell_m = \Phi_{i1}, \tag{19}$$

whose solution is given by

$$\ell_n = \sum_i A_{ni}^+ \Phi_{i1}. \tag{20}$$

Note that although A is invertible, with $A^+ = A^{-1}$, we use the pseudo-inverse notation since we intend to apply the ensuing inversion formula as an approximation under more general conditions.

We now exhibit the cancellations in the IBS. We begin from Eq. (18) and make use of the Born series Eq. (4) for $T[V]$. This results in

$$\sum_m A_{im}v_m = \Phi_{i1} - \sum_m [A(VGV + VGVGV + \cdots)]_{im}$$

$$= \Phi_{i1} - \sum_{n,m} A_{in}(VGV + VGVGV + \cdots)_{nm}. \tag{21}$$

Since A is invertible, Eq. (21) implies that

$$v_n = \ell_n - \sum_m (VGV + VGVGV + \cdots)_{nm}. \tag{22}$$

We now iterate this equation to generate the IBS. At first order, we have $V^{(1)} = L$. At second order, we find the relation

$$v_n^{(2)} = -\sum_m (\mathtt{LGL})_{nm} = -\ell_n \sum_m G_{nm}\ell_m = -\ell_n S_n, \quad \textbf{(23)}$$

where

$$S_n = \sum_m G_{nm}\ell_m. \quad \textbf{(24)}$$

At third order, three terms are found:

$$v_n^{(3a)} = -\sum_m (\mathtt{LGLGL})_{nm} = -\ell_n \sum_m G_{nm}\ell_m S_m, \quad \textbf{(25a)}$$

$$v_n^{(3b)} = -\sum_m (\mathtt{LGV}^{(2)})_{nm} = \ell_n \sum_m G_{nm}\ell_m S_m, \quad \textbf{(25b)}$$

$$v_n^{(3c)} = -\sum_m (\mathtt{V}^{(2)}\mathtt{GL})_{nm} = \ell_n S_n^2. \quad \textbf{(25c)}$$

The rules to calculate the higher-order terms are given in [19]. We immediately see that $\mathtt{V}^{(3a)}$ and $\mathtt{V}^{(3b)}$ cancel and therefore $\mathtt{V}^{(3)} = \mathtt{V}^{(3c)}$. Detailed calculations (not shown here) demonstrate that the same pattern continues at higher orders, with $2^{p-1} - 1$ terms at order p canceling in pairs, resulting in one term. Thus, an exponentially large number of terms at each order of the IBS is replaced by a single term.

We have seen that for the case of a single detector, cancellations in the inverse Born series arise with one term surviving at each order. More generally, such cancellations should not be expected to occur. Nevertheless, we can define the reduced inverse Born series (rIBS) to be of the form of Eq. (15) in which

$$\mathtt{V}_{nm}^{(p)} = v_n^{(p)}\delta_{nm}, \quad \text{where} \quad v_n^{(p)} = \ell_n(-S_n)^{p-1}, \quad \textbf{(26)}$$

as an approximation to the IBS. Evidently, the definition above agrees with Eq. (25c) when $p = 3$.

We will see that, in some instances, the approximation is quite accurate. In particular, if the cancellations are exact, then Eq. (26) agrees with Eq. (16) (and similar expressions obtained at higher orders). It is important to note that the computational cost to implement the rIBS is low. Computing $\mathcal{K}^+$ by a direct method has computational complexity $O(N^3)$ but only one such operation is required. Computing all S_n according to Eq. (24) has complexity $O(N^2)$ and is also performed once.

We now show that the rIBS can be recovered from a nonperturbative inversion formula for the case of a single detector. To proceed, we begin from Eq. (18) and use the invertibility of $\mathtt{A}$ to obtain

$$\sum_m T_{nm}[\mathtt{V}] = \ell_n. \quad \textbf{(27)}$$

Next, making use of the relation $T_{nm} = v_n\delta_{nm} + v_n(\mathtt{VGT})_{nm}$, and carrying out the summation over m, we find that

$$\ell_n = v_n + v_n \sum_m G_{nm}\ell_m. \quad \textbf{(28)}$$

Solving the above equation for v_n, we obtain the inversion formula

$$v_n = \frac{\ell_n}{1 + \sum_m G_{nm}\ell_m} = \frac{\ell_n}{1 + S_n}, \quad \textbf{(29)}$$

where S_n is defined in Eq. (24). We can expand the above solution for v_n in a power series of the form

$$v_n = \ell_n \sum_{p=0}^{\infty} (-1)^p S_n^p, \quad \textbf{(30)}$$

which coincides with the rIBS. We note that the case of a single source and N detectors (and invertible $\mathtt{B}$) results in a similar inversion formula.

4. 1D NUMERICAL EXAMPLES

A. Imaging Geometry

In this section, we consider a scatterer consisting of N volume elements of linear size h embedded in 3D space and arranged in a linear chain. Assuming the chain is aligned with the X axis, the coordinates of the centers of the volume elements are $x_n = nh$ and $y_n = z_n = 0$, where $n = 1, 2, 3, \ldots, N$. Each volume element is assigned a permittivity ϵ_n. We aim to reconstruct all ϵ_n from measurements, assuming the illuminating field, the detection scheme, and the Green's function $\mathtt{G}$ are known.

In the geometry considered, the diagonal elements of $\mathtt{V}$ are related to ϵ_n by [26]

$$v_n = \frac{h^3\chi_n}{1 - (kh)^2(\xi + ikh)\chi_n}, \quad \textbf{(31)}$$

where

$$\chi_n = \frac{\epsilon_n - 1}{4\pi} \quad \textbf{(32)}$$

is the susceptibility and $k = \omega/c$ is the free space wave number. In addition, the numerical constant ξ is given by

$$\xi = \ln(26 + 14\sqrt{3}) - \pi/2 \approx 2.38. \quad \textbf{(33)}$$

Note that there is a one-to-one correspondence between ϵ_n, χ_n, and v_n. In particular, we have

$$\chi_n = \frac{v_n/h^3}{1 + (kh)^2(\xi + ikh)v_n/h^3}, \quad \epsilon_n = 1 + 4\pi\chi_n. \quad \textbf{(34)}$$

In the reconstructions below, we display χ_n rather than ϵ_n, as the former quantity is a convenient measure of the scatterer contrast relative to the vacuum.

The free-space Green's function in 3D [21] is given by

$$G(\mathbf{r}, \mathbf{r}') = k^2 \frac{e^{ik|\mathbf{r}-\mathbf{r}'|}}{|\mathbf{r} - \mathbf{r}'|}. \quad \textbf{(35)}$$

The corresponding matrix $\mathtt{G}$ is obtained by discretization of $G(\mathbf{r}, \mathbf{r}')$. As mentioned above, we use the discretization scheme in which the diagonal of $\mathtt{G}$ is zero, which is consistent with the presence of the denominator in Eq. (31). The resulting expression for the matrix elements of $\mathtt{G}$ is

$$G_{nm} = (1 - \delta_{nm})k^2 \frac{e^{ikh|n-m|}}{h|n-m|}, \quad 1 \leq n, m \leq N. \quad \textbf{(36)}$$

Note that this discretization is specific to the 1D scatterer considered in this section.

To compare the various contrasts and thus the various strengths of nonlinearity in the ISP, we take $\chi_n = \gamma \tilde{\chi}_n$ where γ is a dimensionless positive constant and the nonzero elements $\tilde{\chi}_n$ are of the order of unity. We refer to $\tilde{\chi}_n$ as the model. By changing γ, we can control the degree of nonlinearity in the ISP while keeping the model shape constant. The numerical reconstructions yield the elements of $\mathbb{V}$, v_n, from which we compute χ_n according to Eq. (34). We then compute $\tilde{\chi}_n$ as χ_n/γ. The reconstructed values of $\tilde{\chi}_n$ are displayed in all plots below. Note that the model used in this paper is purely real but the reconstructions generally yield complex values. In the plots, we display only the real parts of $\tilde{\chi}_n$ and ignore the imaginary parts.

Although we display $\tilde{\chi}_n$ in all plots, the error of reconstruction is defined differently. Since we reconstruct directly the values of v_n, we quantify the normalized ℓ^2 error as

$$\eta^2 = \frac{\sum_{n=1}^{N_v} |v_n^{(\mathrm{rec})} - v_n^{(\mathrm{mod})}|^2}{\sum_{n=1}^{N_v} |v_n^{(\mathrm{mod})}|^2}, \tag{37}$$

where (mod) and (rec) refer to the model and reconstructed values.

## B. Incident Plane Waves with an Integrating Detector

We now display numerical results under the same conditions for which the rIBS and the nonperturbative inversion formula Eq. (29) were derived in Section 3. Namely, we consider a formally determined ISP with N degrees of freedom, N distinct plane wave sources, and one integrating detector. We select the illuminating fields so that the linearized ISP is well-posed. To this end, we take the set of incident plane waves that coincide with the Fourier modes of the scatterer. This illumination and detection scheme is described by the following measurement matrices:

$$A_{in} = e^{iq_i x_n}, \qquad B_{m1} = 1, \tag{38}$$

where $1 \leq n, m \leq N, -M \leq i \leq M$ and

$$M = (N - 1)/2. \tag{39}$$

In the numerical examples, we take N to be odd so that M is an integer. These measurement matrices in Eq. (38) are realized if the free-space wave number is $k = \pi/h$ and we illuminate the chain at different angles θ_i. It can be seen that, by using
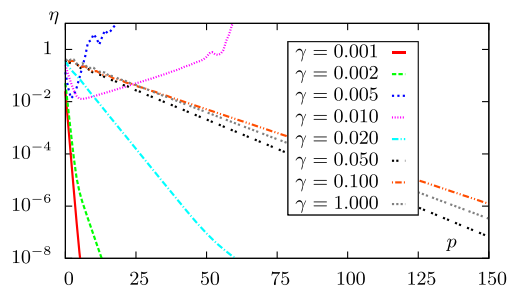
Fig. 1. Convergence of the NK method with iteration order p for different values of the contrast γ for the measurement setup of Section 4.B. Wave number $k = \pi/h$.
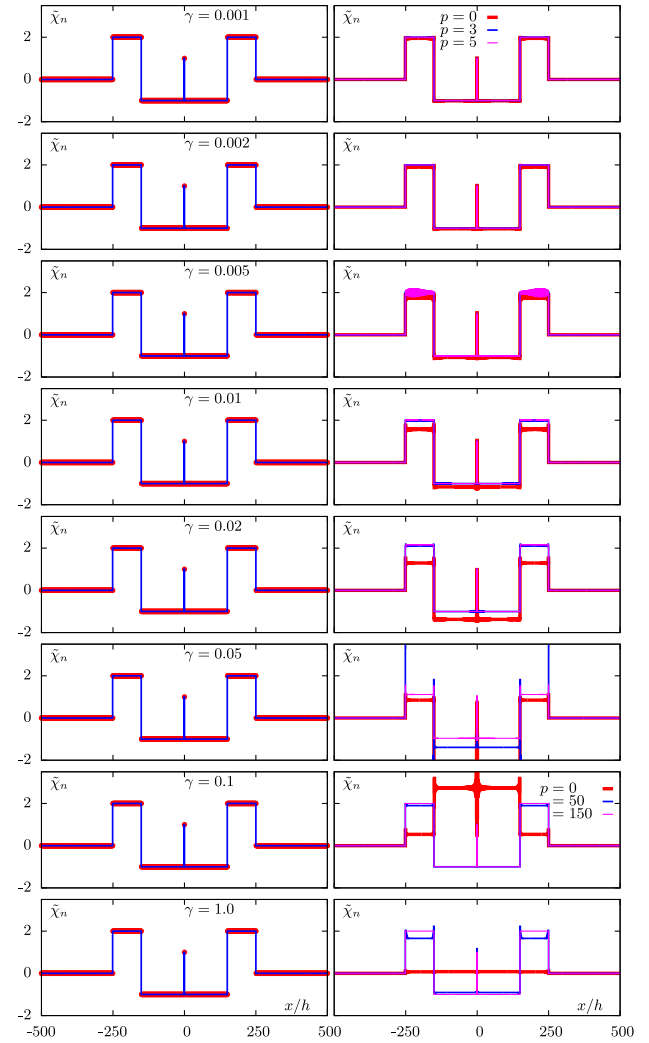
Fig. 2. The reconstructions for the setup of Section 4.B and various contrasts γ. Left: The model (red circles) and reconstructions by the nonperturbative formula Eq. (29) (blue lines). The central peak of the model consists of only one voxel. Right: Reconstructions obtained at various orders p of the NK iterations (order $p = 0$ shown by thick red line corresponds to the linearized reconstruction). Intermediate blue lines show order $p = 3$ for $\gamma \leq 0.05$ and $p = 50$ for $\gamma > 0.05$. Thin magenta lines show order $p = 5$ for $\gamma \leq 0.05$ and $p = 150$ for $\gamma > 0.05$. Wave number $k = \pi/h$.

$$q_i = k \cos \theta_i \quad \text{where} \quad \cos \theta_i = \frac{2i}{N}, \quad x_n = nh, \quad k = \frac{\pi}{h}, \tag{40}$$

we obtain

$$A_{in} = e^{i\frac{2\pi}{N} in}, \tag{41}$$

which is the matrix of the discrete Fourier transform of length N.

We perform reconstructions for a model with $N = 1001$ degrees of freedom consisting of several step functions of varying width. The central peak of the model is one volume element wide. To reconstruct this feature, all Fourier components up to the theoretical band limit are needed. We illustrate convergence of the NK method in Fig. 1. The model and reconstructions by various methods are displayed in Fig. 2.

Table 1. Summary of the Reconstruction Results for the Setup of Section 4.B and Different Values of the Contrast γ [a]

γ	w	η Linearized	η Eq. (29)	NK
0.001	0.037	0.025	$\sim10^{-15}$	Yes
0.002	0.077	0.051	$\sim10^{-15}$	Yes [?]
0.005	0.20	0.13	$\sim10^{-15}$	No
0.01	0.35	0.25	$\sim10^{-15}$	No
0.02	0.50	0.37	$\sim10^{-15}$	Yes [?]
0.05	0.50	0.40	$\sim10^{-15}$	Yes
0.1	0.49	0.41	$\sim10^{-15}$	Yes
1.0	0.47	0.42	$\sim10^{-15}$	Yes

[a]Second column gives the values of w [defined in Eq. (42)]. Third column is the error of linearized inversion as defined in Eq. (37). Fourth column is the error of nonperturbative solution in Eq. (29). Fifth column indicates whether the NK iterations converge. A question mark means that for this particular value of γ we are not certain about convergence.

The results of Fig. 1, where we plot the reconstruction error η as a function of the order of the NK iterations for different values of the contrast γ, are somewhat unexpected. At small values of γ, the NK method converges exponentially. However, for $\gamma = 0.005$ and $\gamma = 0.01$, after a small initial region of convergence, the error begins to accumulate. For even larger values of γ, the NK method again converges exponentially. This is particularly unexpected because the rIBS converges for all values of γ considered. This point is illustrated in Table 1, where we summarize the reconstruction results. In particular, for each γ, we show the quantity

$$w = \max_n |S_n|, \tag{42}$$

where S_n is defined in Eq. (24); here, the index n labels the volume elements. If $w < 1$, the rIBS as given by Eq. (30) converges. We thus have an example in which the rIBS converges but the NK method does not.

The observation above can be explained as follows. When all methods converge, the limit of the NK iterations, when carried out to infinite order, formally coincides with the IBS and, under the conditions of this subsection, with the rIBS. However, the NK iterates do not coincide with the terms of the IBS. A given NK iterate may contain terms with different numbers of factors of L, whereas a given order of the IBS contains only terms with the same number of such factors. Cancellation of terms occurs at each order of the IBS, but not in each order of the NK method. Thus, at any finite order, the NK method generates exponentially many terms, which are not small and not canceled. Therefore, at any finite order, the NK iterates do not coincide with the terms of the rIBS, in which the cancellations have been accounted for analytically.

We now turn to the reconstructions. The left column of images in Fig. 2 shows the model superimposed with the result of the nonperturbative inversion formula Eq. (29), which also coincides with the limit of the rIBS. It can be seen that Eq. (29) works perfectly at all values of γ. The right column shows the linearized reconstructions and various orders of the NK iterations. For relatively small values of γ, the orders $p = 3$ and $p = 5$ are shown, whereas for $\gamma = 0, 1$ and $\gamma = 1.0$, the orders $p = 50$ and $p = 150$ are shown. It can be seen that the NK iterations converge to the correct solution except for $\gamma = 0.005$ and

$\gamma = 0.01$. In the latter two cases, an accurate result is achieved at some a priori unknown order. However, continuing the iterations past this order will result in an accumulation of errors. The convergence of the NK method is slow at larger contrast, with hundreds of steps required to achieve an accurate result. However, the nonperturbative formula yields the solution with machine precision in negligible computation time.

C. Excitation and Detection with Plane Waves (Full Bandwidth)

Next we consider a measurement scheme with the same number of plane wave sources as the number of detectors. The measurement matrices in this case are of the form

$$A_{in} = e^{iq_i x_n}, \qquad B_{mj} = e^{ix_m q_j}, \tag{43}$$

where $1 \leq n, m \leq N$, $-L \leq i, j \leq L$, and q_i are defined in Eq. (40). However, unlike in the previous subsection, where we took $L = M = (N-1)/2$ and $k = \pi/h$, here we take $L = M/2 = (N-1)/4$ and $k = \pi/2h$ (N is selected so that L is an integer). We therefore have

$$A_{in} B_{nj} = e^{i\frac{2\pi}{N}(i+j)n}. \tag{44}$$

Since $i + j$ takes all values in the interval $[-\frac{N-1}{2}, \frac{N-1}{2}]$, the exponentials above include all discrete Fourier modes of the scatterer. The corresponding linearized ISP is overdetermined with $(2L+1)^2 = (N+1)^2/4$ distinct measurements and only N unknowns. The operator $\mathcal{K}$ in this case is not invertible. However, we still have the property $\mathcal{K}^+\mathcal{K} = I$ (while $\mathcal{K}\mathcal{K}^+ \neq I$). Under these conditions, the derivation of the IBS in Section 2.D involves no approximations. On the other hand, the conditions under which the rIBS was derived in Section 3 are not met, and therefore the rIBS yields only an approximate solution in this instance.

In the simulations, we take $N = 1001$, as above; correspondingly, $L = 250$. The convergence of the NK method is illustrated in Fig. 3 and the reconstructions are shown in Fig. 4. A summary of the reconstruction results is given in Table 2. Additionally, we compare the errors of reconstruction for the IBS, the rIBS, and the NK method directly in Table 3.

The findings can be summarized as follows. First, when the NK method converges, it yields a superior result because the solution is found with machine precision. However, starting from $\gamma = 0.02$ (which is a fairly low contrast), the NK iterations diverge and are therefore not useful to solve the problem. At the same time, the rIBS and its theoretical limit Eq. (29) yield an
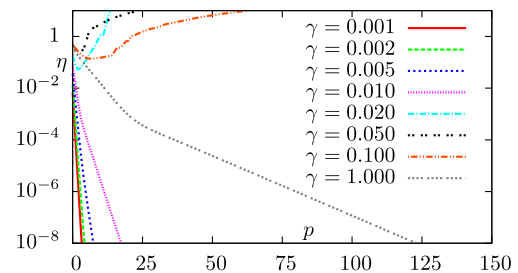
Fig. 3. Convergence of the NK method with iteration order p for different values of the contrast γ for the measurement setup of Section 4.C. Wave number $k = \pi/2h$.
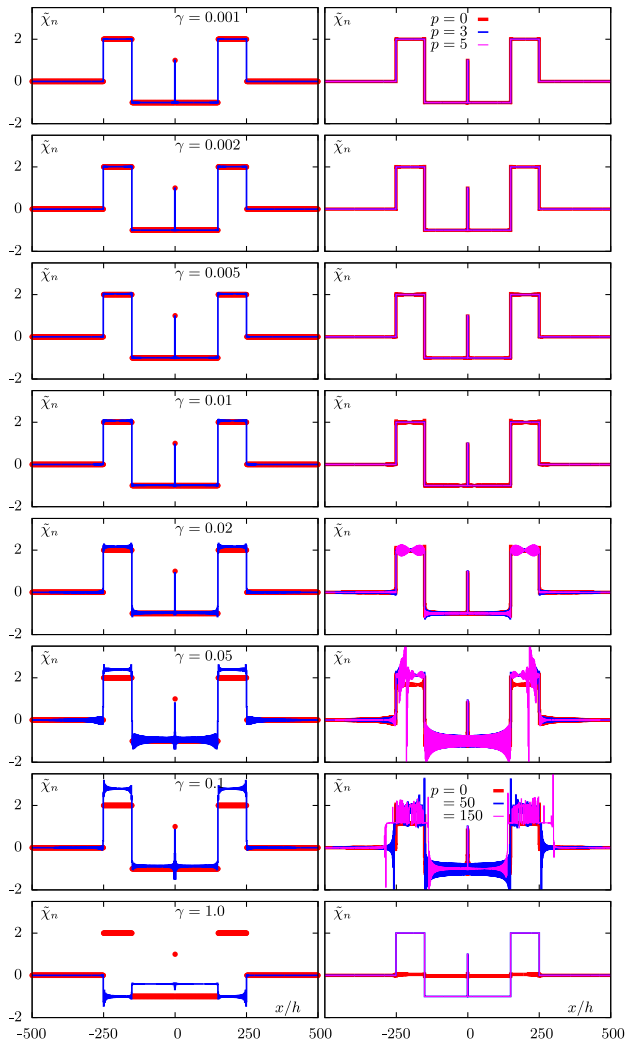
Fig. 4. Same as in Fig. 2, but for the setup of Section 4.C. Wave number $k = \pi/2h$.

Table 2. Summary of the Reconstruction Results for the Setup of Section 4.C and Different Values of the Contrast γ[a]

γ	w	η Linearized	η Eq. (29)	NK
0.001	0.001	0.007	0.003	Yes
0.002	0.02	0.01	0.007	Yes
0.005	0.06	0.04	0.02	Yes
0.01	0.12	0.08	0.04	Yes
0.02	0.25	0.18	0.11	No
0.05	0.61	0.47	0.35	No
0.1	0.65	0.51	0.30	No
1.0	0.50	0.42	0.17	Yes

[a]Same columns as in Table 1.

approximate, yet still a useful, result for values of γ up to $\sim$0.1; only at $\gamma \sim 1$ the rIBS method breaks down completely. The IBS was computed to fifth order. It is either similar to or outperforms the rIBS at each finite order, albeit not by much, but cannot be computed to significantly higher orders than $p = 5$ due to the high computational cost.

Table 3. Reconstruction Error η of IBS, rIBS, and NK Iterations in the Setup of Section 4.C, for Two Values of γ as Labeled[a]

Order p	IBS	rIBS	NK
	$\gamma = 0.01$		
1	$7.9 \cdot 10^{-2}$	$7.9 \cdot 10^{-2}$	$7.9 \cdot 10^{-2}$
2	$9.0 \cdot 10^{-3}$	$9.0 \cdot 10^{-3}$	$1.4 \cdot 10^{-2}$
3	$1.2 \cdot 10^{-3}$	$3.2 \cdot 10^{-3}$	$2.6 \cdot 10^{-3}$
4	$1.7 \cdot 10^{-4}$	$2.9 \cdot 10^{-3}$	$6.9 \cdot 10^{-4}$
5	$3.1 \cdot 10^{-5}$	$3.0 \cdot 10^{-3}$	$2.6 \cdot 10^{-4}$
∞	N/A	$3.0 \cdot 10^{-3}$	$\sim 10^{-15}$
	$\gamma = 0.1$		
1	0.51	0.51	0.51
2	0.29	0.29	0.35
3	0.18	0.20	0.26
4	0.12	0.17	0.20
5	0.11	0.15	0.15
∞	N/A	Diverges	Diverges

[a]The order ∞ corresponds to either the analytical summation or converged result after many iterations. N/A in the IBS columns indicates that the series could not be computed to high orders due to computational complexity.

Table 4. Reconstruction Error η of IBS, rIBS, and NK Iterations in the Setup of Section 4.D, for Two Values of γ as Labeled[a]

Order p	IBS	rIBS	NK
	$\gamma = 0.01$		
1	$7.5 \cdot 10^{-2}$	$7.5 \cdot 10^{-2}$	$6.5 \cdot 10^{-2}$
2	$6.4 \cdot 10^{-2}$	$6.4 \cdot 10^{-2}$	$6.4 \cdot 10^{-2}$
3	$6.4 \cdot 10^{-2}$	$6.4 \cdot 10^{-2}$	$6.4 \cdot 10^{-2}$
4	$6.4 \cdot 10^{-2}$	$6.4 \cdot 10^{-2}$	$6.4 \cdot 10^{-2}$
5	$6.4 \cdot 10^{-2}$	$6.4 \cdot 10^{-2}$	$6.4 \cdot 10^{-2}$
∞	N/A	$6.4 \cdot 10^{-2}$	$6.4 \cdot 10^{-2}$
	$\gamma = 0.1$		
1	0.62	0.62	0.62
2	0.43	0.43	0.57
3	0.31	0.28	0.60
4	0.26	0.17	0.74
5	0.24	0.14	1.06
∞	N/A	0.16	Diverges

[a]Same columns as in Table 3.

D. Excitation and Detection with Plane Waves (Reduced Bandwidth)

Here, we work with the same geometry as in Section 4.C, except that we now take L smaller than $(N - 1)/4$, which is required for the condition $\mathcal{K}^+\mathcal{K} = I$ to hold. Specifically, for $N = 1001$, we take $L = 150$. The wave number is still $k = \pi/2h$. In this case, the exponentials in Eq. (44) represent only 601 out of the total of 1001 Fourier modes of the scatterer. The linearized ISP is underdetermined, and the conditions under which the NK, the IBS, and the rIBS methods were derived do not hold. All these methods can be expected to yield only approximate solutions, and the quality of the approximation is not known a priori. Nevertheless, some improvement compared to the linearized reconstructions can be achieved with the IBS. To

support this conclusion, we show some results of numerical reconstructions in Table 4 (graphical information provides no additional insights). At $\gamma = 0.01$, the linearized reconstruction (order $p = 1$) is reasonably accurate with an error of the order $\eta \sim 0.1$. No meaningful improvement over this result can be achieved by any method. At $\gamma = 0.1$, the IBS achieves a twofold improvement over the linearized reconstruction at the fifth order. Neither the rIBS nor the NK method are of use.

5. 2D NUMERICAL EXAMPLES

A. Imaging Geometry

The transition from 1D to 2D does not entail any conceptual or mathematical difficulties. However, some details must be mentioned. First, the scatterer in this section is an $N \times N$ square lattice embedded in a 3D space. The ISP is to reconstruct the susceptibilities $\chi_{n_x n_y}$ of all $N_v = N^2$ volume elements. Here, instead of a single index n, which takes values from 1 to N^2, we have introduced a composite index $(n_x n_y)$. Assuming the scatterer lies in the XY plane, the coordinates of the centers of the volume element can be written as $\boldsymbol{\rho}_{n_x n_y} = h(n_x \hat{\mathbf{x}} + n_y \hat{\mathbf{y}})$. The model is defined similarly to the 1D case with several overlapping regions. The dimensionless constant γ is used to control the degree of nonlinearity in the ISP. Second, the measurements we consider use incoming and outgoing plane waves, which coincide with some or all Fourier modes of the scatterer. The corresponding measurement matrices are

$$A_{i_x i_y, n_x n_y} = e^{i\mathbf{q}_{i_x i_y} \cdot \boldsymbol{\rho}_{n_x n_y}}, \quad B_{m_x m_y, j_x j_y} = e^{i\mathbf{q}_{j_x j_y} \cdot \boldsymbol{\rho}_{m_x m_y}}, \tag{45}$$

where the 2D wave vectors $\mathbf{q}_{i_x i_y}$ are of the form

$$\mathbf{q}_{i_x i_y} = \frac{2\pi}{Nh}(i_x \hat{\mathbf{x}} + i_y \hat{\mathbf{y}}), \tag{46}$$

and the indexes are sampled as described below, but in all cases satisfy the inequality

$$-\frac{N-1}{2} \le i_x, i_y, j_x, j_y \le \frac{N-1}{2}. \tag{47}$$

Note that we still assume that N is odd. The 2D wave vectors $\mathbf{q}_{i_x i_y}$ are projections of the 3D wave vector $\mathbf{k}$ (of fixed length k) onto the XY plane. Geometrically, this is possible by taking

$$k = \frac{\sqrt{2}\pi}{h} \tag{48}$$

and

$$\mathbf{q}_{i_x i_y} = k \sin \theta_{i_x i_y} (\hat{\mathbf{x}} \cos \phi_{i_x i_y} + \hat{\mathbf{y}} \sin \phi_{i_x i_y}). \tag{49}$$

We will use the wave number defined in Eq. (48) throughout this section, unlike in the 1D examples of Section 4 where different values of k were used in different examples. The rotation angles can be determined from

$$\sin^2 \theta_{i_x i_y} = \frac{2(i_x^2 + i_y^2)}{N^2}, \quad \cos \phi_{i_x i_y} = \frac{i_x^2}{i_x^2 + i_y^2}. \tag{50}$$

Third, the discretized Green's function is now a slight generalization of Eq. (36):

$$G_{n_x n_y, m_x m_y} = (1 - \delta_{n_x n_y, m_x m_y}) \frac{k^2 e^{ik|\boldsymbol{\rho}_{n_x n_y} - \boldsymbol{\rho}_{m_x m_y}|}}{|\boldsymbol{\rho}_{n_x n_y} - \boldsymbol{\rho}_{m_x m_y}|}. \tag{51}$$

Here, the Kronecker delta symbol $\delta_{n_x n_y, m_x m_y}$ is 1 if $n_x = m_x$ and $n_y = m_y$ simultaneously and 0 otherwise. The wave number k in Eq. (51) is the same as is given in Eq. (48). Finally, it should be noted that, for 2D scatterers, the interaction of volume elements is stronger than in the 1D case due to more dense packing. Therefore, somewhat smaller values of γ are considered below.

B. Incident Plane Waves with an Integrating Detector

We first consider the case when the derivation of the rIBS involves no approximations. To this end, we take $N = 51$ ($N_v = 2601$ degrees of freedom), and use incident waves with the wave vectors $\mathbf{q}_{i_x i_y}$ with the indexes satisfying $-M \le i_x, i_y \le M$, where M is defined in Eq. (39). We therefore use $N_s = 2601$ incident plane waves ($N_s = N_v$), which sample all Fourier modes of the scatterer. We also use a single integrating detector. In this setting, the conditions of the derivation of the rIBS and of the nonperturbative formula Eq. (29) are met. However, as mentioned above, the nonlinearity of the ISP now sets in for much smaller contrast γ compared to the 1D case. We therefore consider the relatively small values $\gamma = 0.001$ and $\gamma = 0.01$.

Reconstructions are shown in Fig. 5, and the relevant numerical data are summarized in Table 5. For $\gamma = 0.001$, both the NK method and the rIBS converge to the exact result. The IBS in this case yields numerical values equivalent to those of the rIBS but is harder to compute. For $\gamma = 0.01$, neither of
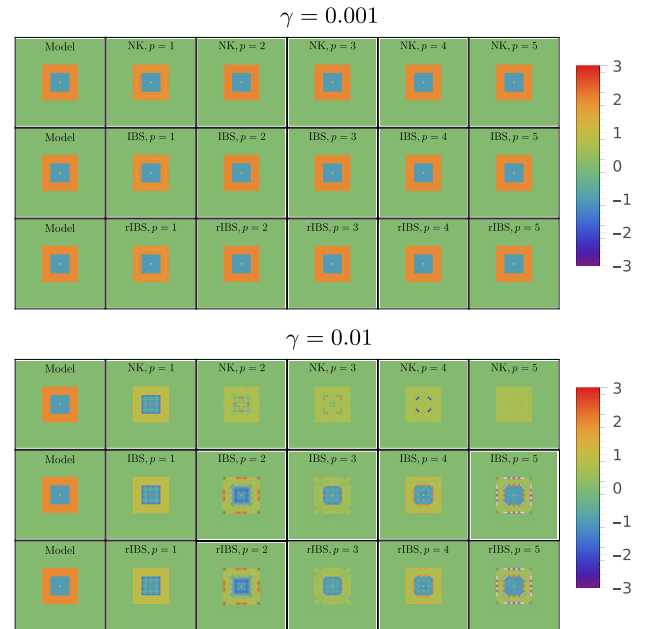
Fig. 5. The reconstructions for the 2D measurement setup of Section 5.B for $\gamma = 0.001$ and $\gamma = 0.01$. Note that, even though all expansions or iterative methods diverge for $\gamma = 0.01$, the nonperturbative formula Eq. (29) is exact. This result is not shown in the figure because the corresponding reconstruction coincides with the model with machine precision. Wave number $k = \sqrt{2}\pi/h$.

Table 5. Reconstruction Error η for the Setup of Section 5.B [a]

Order p	IBS	rIBS	NK
	$\gamma = 0.001\ (w = 0.21)$		
1	0.11	0.11	0.11
2	$1.67 \cdot 10^{-2}$	$1.67 \cdot 10^{-2}$	$2.87 \cdot 10^{-2}$
3	$2.78 \cdot 10^{-3}$	$2.78 \cdot 10^{-3}$	$7.48 \cdot 10^{-3}$
4	$4.98 \cdot 10^{-4}$	$4.98 \cdot 10^{-4}$	$1.96 \cdot 10^{-3}$
5	$9.34 \cdot 10^{-5}$	$9.34 \cdot 10^{-5}$	$5.25 \cdot 10^{-4}$
∞	$\sim 10^{-15}$	$\sim 10^{-15}$	$\sim 10^{-15}$
	$\gamma = 0.01\ (w = 2.36)$		
1	1.47	1.47	1.47
2	2.69	2.69	5.64
3	5.36	5.36	9.99
4	11.24	11.24	12.43
5	24.29	24.29	15.19
∞	Diverges	Diverges	Diverges

[a]Same columns as in Table 3. In addition to γ, the value of w defined in Eq. (42) is shown. Note that, for $w \geq 1$, rIBS diverges.

the iterative methods converge. The nonperturbative formula Eq. (29), however, still yields the exact result. Reconstructions performed according to Eq. (29) are not shown in Fig. 5 because they coincide with the model. We thus see that, in the regime of strong nonlinearity, the IBS, rIBS, or iterative methods are not effective even under the strong assumptions of this subsection. The nonperturbative formula, however, remains useful.

C. Excitation and Detection with Plane Waves (Full Bandwidth)

We next consider a measurement scheme in which identical sets of incident and outgoing plane waves are used for illumination and detection. Each set is the same as the set of incident waves used in Section 5.B. Thus, the linearized ISP is strongly overdetermined, with $N_s = N_d = N_v$. However, we still have $\mathcal{K}^+ \mathcal{K} = \mathsf{I}$. Under this condition, the NK method and the IBS, if convergent, yield the exact result. However, the conditions under which the rIBS was derived are not met and the latter can be viewed as an approximation.

Reconstructions are shown in Fig. 6 and the relevant numerical data are summarized in Table 6. At $\gamma = 0.01$, the linearized solution is close to the model and no further improvement can be obtained by the expansion methods. In particular, IBS diverges. The rIBS converges to the theoretical limit Eq. (29); however, the latter contains a noticeable error, but is still good quality visually. However, the NK iterations converge to the exact result almost with machine precision. A qualitatively similar picture emerges at a larger value of the contrast $\gamma = 0.1$. The IBS diverges but the rIBS converges to a result that is not far off from the model. The NK iterations still yield the correct reconstruction with machine precision. It can be concluded that the NK method is superior in this case, but it is much harder to compute than rIBS or the nonperturbative formula Eq. (29), which both yield reasonable results. Under the conditions of this subsection, the rIBS provides a useful approximation.

Finally we note that both measurement matrices A and B used in this subsection are invertible. In this case, the ISP can be solved analytically by three matrix inversions. Indeed, we
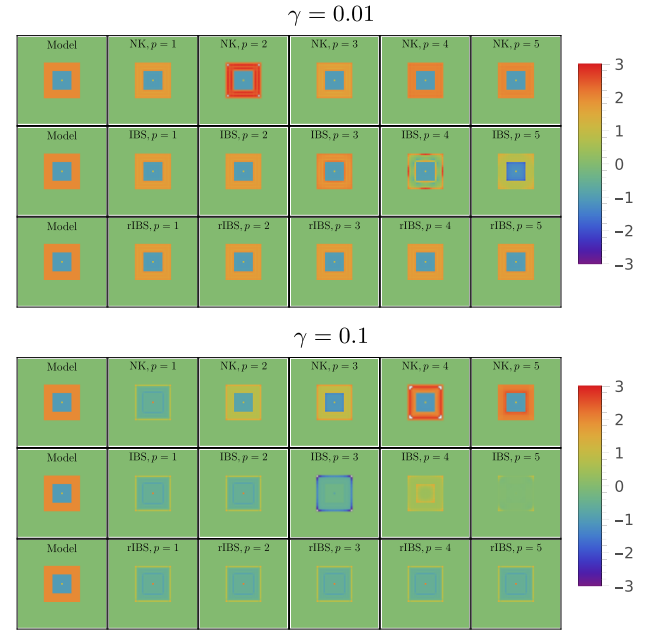
Fig. 6. The reconstructions for the 2D measurement setup of Section 5.C for $\gamma = 0.01$ and $\gamma = 0.1$. Wave number $k = \sqrt{2}\pi/h$.

Table 6. Reconstruction Error η for the Setup of Section 5.C [a]
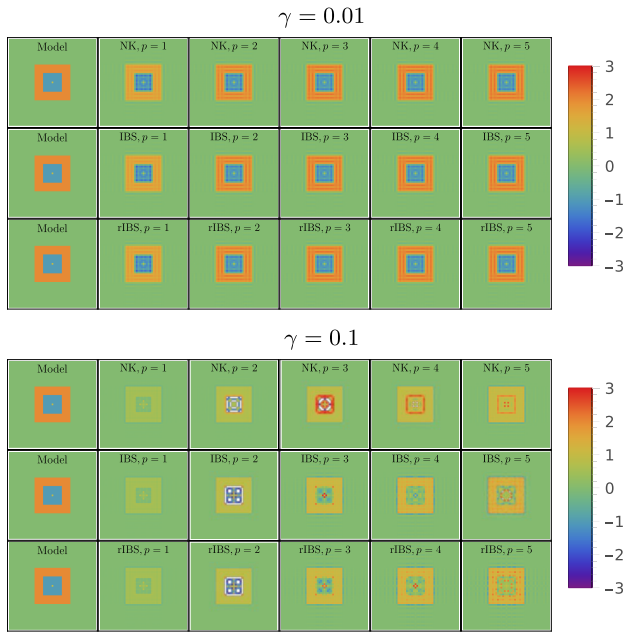
Order p	IBS	rIBS	NK
	$\gamma = 0.01$		
1	0.15	0.15	0.15
2	0.15	0.15	0.13
3	0.12	0.15	0.095
4	0.44	0.15	0.061
5	0.91	0.15	0.049
∞	Diverges	0.15	$\sim 10^{-15}$
	$\gamma = 0.1$		
1	0.11	0.11	0.11
2	0.11	0.11	0.061
3	0.19	0.11	0.042
4	0.17	0.11	0.025
5	0.62	0.11	0.014
∞	N/A	0.11	$\sim 10^{-15}$

[a]Same columns as in Table 3.

can find T from Eq. (5) by acting with A^{-1} and B^{-1} and then find the solution as $\mathsf{V} = (\mathsf{I} + \mathsf{T}\mathsf{G})^{-1}\mathsf{T}$. A family of methods that find V as the minimum norm solution (in case the latter equation does not yield a diagonal matrix) is also easily derivable. However, ISPs with this property are rarely encountered in practice.

D. Reduced Bandwidth

We consider an $N \times N$ scatterer with $N = 51$, but now the incident and outgoing waves sample the Fourier modes of the scatterer only within a reduced band limit. The indexes of the wave vectors of the incoming and outgoing waves $\mathbf{q}_{i_x i_y}$ and $\mathbf{q}_{j_x j_y}$ are now limited by the condition $-L \leq i_x, i_y, j_x, j_y \leq L$,

$$\gamma = 0.01$$

$$\gamma = 0.1$$

Fig. 7.   The reconstructions for the 2D measurement setup of Section 5.D for $\gamma = 0.01$ and $\gamma = 0.1$. Wave number $k = \sqrt{2}\pi/h$.

Table 7.   Reconstruction Error η for the Setup of Section 5.D[a]

Order p	IBS	rIBS	NK
		$\gamma = 0.01$	
1	0.30	0.30	0.30
2	0.18	0.18	0.20
3	0.17	0.17	0.17
4	0.17	0.17	0.17
5	0.91	0.17	0.17
∞	Diverges	0.17	0.17
		$\gamma = 0.1$	
1	0.84	0.84	0.84
2	0.74	0.74	0.80
3	0.69	0.70	0.80
4	0.66	0.70	0.85
5	0.68	0.75	0.96
∞	N/A	Diverges	Diverges

[a]Same columns as in Table 3.

where $L = 10$. Note that $2L < M$, where $M = 25$ according to the definition Eq. (39). Correspondingly, the product

$$A_{i_x i_y, \, n_x n_y} B_{n_x n_y, \, j_x j_y} = e^{i\frac{2\pi}{N}[(i_x + j_x)n_x + (i_y + j_y)n_y]} \qquad (52)$$

samples the Fourier coefficients of the scatterer only within the band limit $[-2L, 2L] \times [-2L, 2L]$ where $2L = 20$, whereas the complete set of coefficients covers the area $[-M, M] \times [-M, M]$ where $M = 25$. Therefore, 920 out of the total of 2601 Fourier coefficients of the scatterer are not accessible in the linearized ISP, which is in these cases ill-posed. The linearized ISP is still overdetermined, with 10^4 data points and only $N = 2,601$ unknowns. However, many of the linear equations in Eq. (7) are redundant. Correspondingly, $\mathcal{K}^+\mathcal{K} \neq \mathtt{I}$ and the conditions under which all inversion methods used in

this paper were derived are not met. We can still apply these methods and study the quality of the obtained reconstructions.

The reconstructions are shown in Fig. 7, and the relevant numerical data are adduced in Table 7. It can be seen that, at the relatively small contrast corresponding to $\gamma = 0.01$, linearized inversion yields a reasonable result and some small improvement can be achieved by either the rIBS or NK method. The nonperturbative formula Eq. (29) and the fixed point of the NK iterations yield a comparable improvement over linearization. However, at $\gamma = 0.1$, the ISP becomes essentially nonlinear and all methods fail in the sense that no meaningful improvement over the linearized solution (which has a large error but preserves some geometrical information) can be achieved.

6. DISCUSSION

We have considered the ISP for scalar waves in a medium discretized as a set of small cubic volume elements arranged in a 1D structure (chain) or 2D structure (square lattice). We have found conditions under which many terms in the IBS cancel in pairs, leaving only one term at each order. We refer to the resulting expansion as the rIBS. The terms in the reduced series can be resummed, resulting in a nonperturbative inversion formula. This result can also be derived directly, without resumming the series.

The assumptions that led to the results above are rather restrictive. We therefore investigated the rIBS and the nonperturbative inversion formula Eq. (29) beyond their conditions of applicability. It was found that they can often be used as reasonable approximations, especially considering that other methods such as NK or the IBS do not perform better, but are much harder to compute. We emphasize that the overriding advantages of the rIBS and of Eq. (29) is computational efficiency.

An important observation can be made from the numerical examples discussed above. Typically, the linearized ISP must be regularized to avoid numerical instability. The resulting reconstructions have relatively low spatial resolution. However, the generalization of this approach to nonlinear ISPs is not straightforward. For this reason, replacing the inverse of the linearized forward operator $\mathcal{K}^{-1}$ with a pseudo-inverse $\mathcal{K}^+$ in the NK method does not generally lead to a noticeable improvement in resolution. The question of whether it is possible to recover the potential by solving a nonlinear ISP under the condition that $\mathcal{K}^+\mathcal{K} \neq \mathtt{I}$ is rather complicated mathematically and was the subject of a recent computational study [27] with a pessimistic conclusion.

Disclosures.   The authors declare no conflicts of interest.

Data availability.   No data were generated or analyzed in this paper.

REFERENCES

1. D. Colton and R. Kress, _Inverse Acoustic and Electromagnetic Scattering Theory_ (Springer, 2013).
2. E. Wolf, "Three-dimensional structure determination of semi-transparent objects from holographic data," Opt. Commun. **1**, 153 (1969).
3. A. Devaney and E. Wolf, "A new perturbation expansion for inverse scattering from three dimensional finite range potentials," Phys. Lett. A **89**, 269 (1982).
4. H. Moses, "Calculation of the scattering potential from reflection coefficients," Phys. Rep. **102**, 550 (1956).
5. R. Jost and W. Kohn, "Construction of a potential from a phase shift," Phys. Rep. **87**, 977 (1952).
6. R. Prosser, "Formal solutions of the inverse scattering problem," J. Math. Phys. **10**, 1819 (1969).
7. S. Arridge, S. Moskow, and J. C. Schotland, "Inverse Born series for the Calderon problem," Inverse Prob. **28**, 035003 (2012).
8. P. Bardsley and F. G. Vasquez, "Restarted inverse Born series for the Schrodinger problem with discrete internal measurements," Inverse Prob. **30**, 045014 (2014).
9. K. Kilgore, S. Moskow, and J. C. Schotland, "Inverse Born series for scalar waves," J. Comput. Math. **30**, 601 (2012).
10. K. Kilgore, S. Moskow, and J. C. Schotland, "Convergence of the Born series and inverse Born series for electromagnetic scattering," Appl. Anal. **96**, 1737 (2017).
11. M. Machida and J. C. Schotland, "Inverse Born series for the radiative transport equation," Inverse Prob. **31**, 095009 (2015).
12. V. A. Markel, J. A. O'Sullivan, and J. C. Schotland, "Inverse problem in optical diffusion tomography. IV. Nonlinear inversion formulas," J. Opt. Soc. Am. A **20**, 903–912 (2003).
13. M. Moskow and J. Schotland, "Numerical studies of the inverse Born series for diffuse waves," Inverse Prob. **25**, 095007 (2009).
14. G. Y. Panasyuk, V. A. Markel, P. S. Carney, and J. C. Schotland, "Nonlinear inverse scattering and three-dimensional near-field optical imaging," Appl. Phys. Lett. **89**, 221116 (2006).
15. A. B. Weglein, F. V. Araujo, P. M. Carvalho, R. H. Stolt, K. H. Matson, R. T. Coates, R. T. Corrigan, D. Corrigan, D. J. Foster, S. A. Shaw, and H. Zhang, "Inverse scattering series and seismic exploration," Inverse Prob. **19**, R27–R83 (2003).
16. S. Moskow and J. Schotland, "Convergence and stability of the inverse scattering series for diffuse waves," Inverse Prob. **24**, 065005 (2008).
17. F. Chung, A. Gilbert, J. Hoskins, and J. C. Schotland, "Optical tomography on graphs," Inverse Prob. **33**, 055016 (2017).
18. J. Hoskins and J. C. Schotland, "Analysis of the inverse Born series: an approach through geometric function theory," Inverse Prob. **38**, 074001 (2022).
19. S. Moskow and J. C. Schotland, _Inverse Born Series_ (De Gruyter, 2019).
20. P. Deuflhard, _Newton Methods for Nonlinear Problems_ (Springer, 2004).
21. R. Carminati and J. C. Schotland, _Principles of Scattering and Transport of Light_ (Cambridge University, 2021).
22. V. A. Markel, "Extinction, scattering and absorption of electromagnetic waves in the coupled-dipole approximation," J. Quant. Spectrosc. Radiat. Transfer **236**, 106611 (2019).
23. H. W. Levinson and V. A. Markel, "Nonlinear inverse problem by T-matrix completion. I. Theory," Phys. Rev. E **94**, 043317 (2016).
24. V. A. Markel, H. Levinson, and J. C. Schotland, "Fast linear inversion for highly overdetermined inverse scattering problems," Inverse Prob. **35**, 124002 (2019).
25. V. A. Markel and J. C. Schotland, "Symmetries, inversion formulas, and image reconstruction for optical tomography," Phys. Rev. E **70**, 056616 (2004).
26. H. W. Levinson and V. A. Markel, "Solution of the inverse scattering problem by T-matrix completion. II. Simulations," Phys. Rev. E **94**, 043318 (2016).
27. V. A. Markel, "Investigation of the effect of super-resolution in nonlinear inverse scattering," Phys. Rev. E **102**, 053313 (2020).